

**Effect of turbulence on collisional growth of cloud droplets**

XIANG-YU LI\*

*Department of Meteorology and Bolin Centre for Climate Research, Stockholm University, Stockholm, Sweden;  
 Nordita, KTH Royal Institute of Technology and Stockholm University, 10691 Stockholm, Sweden;  
 Swedish e-Science Research Centre, www.e-science.se, Stockholm, Sweden;  
 Laboratory for Atmospheric and Space Physics, University of Colorado, Boulder, CO 80303, USA;  
 JILA and Department of Astrophysical and Planetary Sciences University of Colorado, Boulder, CO 80303, USA*

AXEL BRANDENBURG

*Laboratory for Atmospheric and Space Physics, University of Colorado, Boulder, CO 80303, USA;  
 Nordita, KTH Royal Institute of Technology and Stockholm University, 10691 Stockholm, Sweden;  
 JILA and Department of Astrophysical and Planetary Sciences University of Colorado, Boulder, CO 80303, USA;  
 Department of Astronomy, Stockholm University, SE-10691 Stockholm, Sweden*

GUNILLA SVENSSON

*Department of Meteorology and Bolin Centre for Climate Research, Stockholm University, Stockholm, Sweden;  
 Swedish e-Science Research Centre, www.e-science.se, Stockholm, Sweden;  
 Global & Climate Dynamics, National Center for Atmospheric Research, Boulder, CO 80305, USA*

NILS E. L. HAUGEN

*SINTEF Energy Research, 7465 Trondheim, Norway;  
 Department of Energy and Process Engineering, NTNU, 7491 Trondheim, Norway*

BERNHARD MEHLIG

*Department of Physics, Gothenburg University, 41296 Gothenburg, Sweden*

IGOR ROGACHEVSKII

*Department of Mechanical Engineering, Ben-Gurion Univ. of the Negev, P. O. Box 653, Beer-Sheva 84105, Israel;  
 Nordita, KTH Royal Institute of Technology and Stockholm University, 10691 Stockholm, Sweden*

**ABSTRACT**

We investigate the effect of turbulence on the collisional growth of  $\mu\text{m}$ -sized droplets by high-resolution numerical simulations with well resolved Kolmogorov scales, assuming a collision and coalescence efficiency of unity. The droplet dynamics and collisions are approximated using a superparticle approach. We show that the time evolution of the shape of the droplet-size distribution due to turbulence-induced collision depends strongly on the turbulent energy-dissipation rate, but only weakly on the Reynolds number. The size distribution exhibits power law behavior with a slope of  $-3.7$  in the size range of about  $10 \sim 40 \mu\text{m}$ , which is close to the power law size distribution found for interstellar dust grains. When gravity is invoked, the strong dependency becomes weakened. Turbulence is found to dominate the time evolution of an initially monodisperse droplet distribution at early times. At later times, however, gravity takes over and dominates the collisional growth. With combined turbulence and gravity, the time scale to reach drizzle sized droplets is about 900 s, which is close to the time scale of rapid warm rain formation. The collision rate grows exponentially, which is consistent with the theoretical prediction of the continuous collisional growth even when the turbulence-generated collision is invoked.

---

\* Corresponding author address: Xiang-Yu Li, Department of Meteorology and Bolin Centre for Climate Research, Stockholm University, Stockholm, Sweden

---

E-mail: xiang.yu.li@su.se

## 1. Introduction

Collisional growth of inertial particles in a turbulent environment plays an important role in many physical processes (Pumir and Wilkinson 2016). For instance, collisional growth of droplets in atmospheric clouds may explain the rapid warm rain formation (Shaw 2003). Collisions of dust grains in circumstellar disks is proposed to be a key step towards planet formation (Johansen and Lambrechts 2017).

The most notorious difficulty is how turbulence affects the collisional growth. This problem has a long history and was recently reviewed by Pumir and Wilkinson (2016) and Grabowski and Wang (2013). The pioneering work by Saffman and Turner (1956) proposed a theoretical model for the collision rate (Saffman-Turner model) of cloud droplets. The key idea of the Saffman-Turner model is that the collision rate is dominated by small scales of turbulence since the size of cloud droplets (typical size is  $10\mu\text{m}$  in radius) are three orders of magnitude smaller than the Kolmogorov length (i.e., the smallest scale of turbulence which is about 1 mm in atmospheric clouds). The Saffman-Turner model predicts that the mean collision rate  $\bar{R}_c$  is proportional to the mean energy dissipation rate  $\bar{\epsilon}$  if there is no intermittency and the particle inertia is small.

Due to the rapid advances in computer technology, the collision rate has been studied using direct numerical simulations (DNS). For example, Wang and Grabowski (2009) investigated the collisional growth of cloud droplets by means of combining the parameterized collision process with DNS of turbulence. They concluded that turbulence enhances the collisional growth by a factor of 2. They also found that the Reynolds number dependency is uncertain due to the small Reynolds numbers in their simulations. Onishi and Seifert (2016) updated the collision rate model of Wang and Grabowski (2009) and performed DNS at higher Reynolds number simulations. Onishi and Seifert (2016) found that the collisional growth of cloud droplets depends on Reynolds number. However, they did not study the time evolution of the size distribution and its dependency on Reynolds number and energy dissipation rate.

In fully-developed turbulence, droplet collisions result in a wide range of droplet sizes and thus in a wide range of droplet Stokes numbers that evolve during the simulation. The Stokes number is a dimensionless measure of the effect of droplet inertia, which depends on the geometrical droplet size and the turbulence intensity. In cloud turbulence with  $\bar{\epsilon} \approx 0.04\text{m}^2\text{s}^{-3}$ , the Stokes number  $St$  varies from  $10^{-3}$  (droplet radius of about  $1\mu\text{m}$ ) to 10 (about  $100\mu\text{m}$ ) and beyond. Very small cloud droplets (for  $St \ll 1$ ) are advected by turbulent air flow and the collision is caused by local turbulent shear (Saffman and Turner 1956; Andersson et al. 2007). For larger Stokes numbers, on the

other hand, inertial effects become important, that allow the droplets to detach from the flow. This may substantially increase the collision rate (Sundaram and Collins 1997; Falkovich et al. 2002; Wilkinson et al. 2006). The time-dependent collision rate due to the dynamical Stokes number cannot be captured with a predetermined parameterization of the collision rate. Saito and Gotoh (2017) developed a Lagrangian algorithm to detect the collision without using a parameterized collision kernel. They observed that turbulence broadens the size distribution of cloud droplets. Since their work has condensation included, it is unclear if the broadening of the size distribution results from the turbulence effect on the collisions or its effect on condensation.

Here we determine the droplet-size distribution directly from numerical simulations, thus avoiding the use of a parameterized kernel. We focus on the time evolution of the size distribution due to collisions and how changing the Reynolds number and the energy dissipation rate affect the size distribution. We perform high resolution DNS of turbulence with a well resolved Kolmogorov viscous scale (our maximum Taylor-microscale Reynolds number is 158). Droplet and collision dynamics are solved together using a superparticle approach assuming unit collision and coalescence efficiency. Unit coalescence efficiency means that droplets coalesce upon collision. In the meteorology community, the process of collision and coalescence is referred to as collection, while in the astrophysical community, this process is referred to as coagulation. Since we assume unit coalescence efficiency in the present study, we use the terminology collision. To address the turbulence-facilitated collision for more general applications (such as interstellar dust), we will first focus on DNS without gravity. We will then turn to DNS with both gravity and turbulence, which is important for the cloud droplet formation.

## 2. Numerical setup

Our simulations are conducted using the PENCIL CODE. The DNS of the turbulent flow are performed for a weakly compressible gas, and we adopt a superparticle algorithm to approximate the droplet dynamics (Zsom and Dullemond 2008; Shima et al. 2009; Johansen et al. 2012).

*DNS of the turbulent air flow.* The velocity  $\mathbf{u}$  of the turbulent air flow is determined by the Navier-Stokes equation:

$$\frac{\partial \mathbf{u}}{\partial t} + \mathbf{u} \cdot \nabla \mathbf{u} = \mathbf{f} - \rho^{-1} \nabla p + \rho^{-1} \nabla \cdot (2\nu \rho \mathbf{S}), \quad (1)$$

where  $\mathbf{f}$  is a monochromatic random forcing function (Brandenburg 2001),  $\nu$  is the kinematic viscosity of the air flow,  $S_{ij} = \frac{1}{2}(\partial_j u_i + \partial_i u_j) - \frac{1}{3}\delta_{ij} \nabla \cdot \mathbf{u}$  is the traceless rate-of-strain tensor,  $p$  is the gas pressure, and  $\rho$  is the gas

TABLE 1. Summary of the simulations.

Run	$N_p/10^6$	$N_{\text{grid}}$	$f_0$	$L$ (m)	$u_{\text{rms}}$ ( $\text{m s}^{-1}$ )	$\text{Re}_\lambda$	$\bar{\epsilon}$ ( $\text{m}^2\text{s}^{-3}$ )	$\eta \cdot 10^{-4}$ (m)	$\tau_\eta$ (s)
A	8.4	$256^3$	0.02	0.125	0.17	57	0.039	4	0.016
B	67	$512^3$	0.02	0.25	0.21	94	0.04	4	0.016
C	67	$512^3$	0.02	0.50	0.27	158	0.036	4	0.017
D	67	$512^3$	0.0072	0.44	0.13	98	0.005	7	0.044
E	67	$512^3$	0.01	0.37	0.15	97	0.01	6	0.032
F	67	$512^3$	0.014	0.30	0.18	94	0.02	5	0.022

Here,  $f_0$  is the amplitude of the random forcing (see text) and  $L$  is the domain size.

density, which in turn obeys the continuity equation,

$$\frac{\partial \rho}{\partial t} + \nabla \cdot (\rho u) = 0. \quad (2)$$

We assume that the gas is isothermal with constant sound speed  $c_s$ , so that  $c_s^2 = \gamma p / \rho$ , where  $\gamma = c_p / c_v = 7/5$  is the ratio between specific heats,  $c_p$  and  $c_v$ , at constant pressure and constant volume, respectively. The sound speed is set to  $5 \text{ m s}^{-1}$ , resulting in a Mach number of 0.06 when the  $u_{\text{rms}} = 0.27 \text{ m s}^{-1}$ . We quantify the weak compressibility in our DNS by calculating the dimensionless number  $\beta = \langle |\nabla \cdot u|^2 \rangle / \langle |\nabla \times u|^2 \rangle = 2 \times 10^{-4}$ . Following Gustavsson and Mehlig (2016b),  $\beta$  corresponds to a Stokes number  $St = 0.018$ , below which compressibility may affect the spatial distribution of the droplets. Initially, the smallest Stokes number is  $St = 0.05$  in our DNS. Therefore, compressibility does not have a significant effect on the droplets. To characterize the intensity of turbulence, we use the Taylor microscale Reynolds number  $\text{Re}_\lambda \equiv u_{\text{rms}}^2 \sqrt{5} / (3\nu \bar{\epsilon})$ , where  $u_{\text{rms}}$  is the rms turbulent velocity, and  $\bar{\epsilon} = 2\nu \text{Tr} S_{ij}^T S_{ij}$  is the mean energy-dissipation rate per unit mass and  $\text{Tr}$  denotes the trace. The parameters of all simulations are listed in Table 1. Here  $\tau_\eta = (\nu / \bar{\epsilon})^{1/2}$  is the Kolmogorov time and  $\eta = (\nu^3 / \bar{\epsilon})^{1/4}$  is the Kolmogorov length.

*Superparticle algorithm.* The equations governing the dynamics and collision of droplets in a turbulent flow are solved simultaneously with the Navier-Stokes equations. We approximate the droplet dynamics and collisions using a stochastic Monte Carlo algorithm that represents a number of spherical droplets by a superparticle (Li et al. 2017; Shima et al. 2009; Zsom and Dullemond 2008; Johansen et al. 2012). All droplets in superparticle  $i$  are assumed to have the same material density  $\rho_d$ , radius  $r_i$ , and velocity  $v_i$ . Further, each superparticle is assigned a volume of the grid cell and thus a droplet number density,  $n_i$ . The position  $x_i$  of superparticle  $i$  is determined by

$$\frac{dx_i}{dt} = V_i \quad (3)$$

and

$$\frac{dV_i}{dt} = \frac{1}{\tau_i} (u - V_i) + g. \quad (4)$$

Here,

$$\tau_i = 2\rho_d r_i^2 / [9\rho \nu C(\text{Re}_i)] \quad (5)$$

is the particle response time attributed to superparticle  $i$ . The correction factor (Schiller and Naumann 1933; Marchioli et al. 2008)  $C(\text{Re}_i) = 1 + 0.15 \text{Re}_i^{0.687}$  models the effect of non-zero particle Reynolds number  $\text{Re}_i = 2r_i |u - V_i| / \nu$ . This is a widely used approximation, although it does not correctly reproduce the small- $\text{Re}_i$  correction to Stokes formula (Veysey and Goldenfeld 2007). The dimensionless particle-response time is given by the Stokes number  $St = \tau_i / \tau_\eta$ . Droplets are randomly distributed in the simulation domain with zero velocity initially. The term  $g$  in equation (4) is included only when collisions are also driven by gravity, in addition to turbulence.

Droplet collisions are represented by collisions of superparticles (Johansen et al. 2012). When two superparticles collide, two droplets in either of the superparticles can collide with probability  $p_c = \tau_c^{-1} \Delta t$ , where  $\Delta t$  is the integration time step. A collision event occurs when  $p_c > \eta_c$ , where  $\eta_c$  is a random number. A mean-field model is adopted for the collision time  $\tau_c$ :

$$\tau_c^{-1} = \sigma_c n_j |V_i - V_j| E_c. \quad (6)$$

Here  $\sigma_c = \pi(r_i + r_j)^2$  is the geometric collision cross section between two droplets with radii  $r_i$  and  $r_j$ . The parameter  $E_c$  is the collision efficiency (Devenish et al. 2012). It is set to unity in our simulations, and we assume that the droplets coalesce upon collision. It is worth noting that a cylindrical kernel is used in the present superparticle scheme as described by equation (6). This is in contrast to what is done for Lagrangian point particle simulations (Wang et al. 1998). In those simulations, a spherical kernel was used, where collisions were not enabled. The use of a cylindrical kernel in the superparticle approach is justified because the superparticle approach treats collisions in a statistical fashion, where the interacting superparticles are considered to fill the entire grid cell.

Collisions are enabled at the same time when the simulation starts with  $\mathbf{u} = \mathbf{0}$ . This yields virtually the same result compared to the case when turbulence is already fully developed and droplets are mixed; see appendix 4. Since collisions can only happen when a pair of superparticles resides in the same grid cell, the statistical convergence of initial  $N_p/N_{\text{grid}}$  ( $N_p$  is the number of superparticles and  $N_{\text{grid}}$  is the number of grid cells.) becomes important. Furthermore, to obtain fully developed turbulence, a large number of mesh points  $N_{\text{grid}}$  ( $512^3$  in the present study) is essential. This requires a large number of superparticles, which is computationally expensive even on the modern supercomputers. We investigate the statistical convergence with respect to the initial value of  $N_p/N_{\text{grid}}$  and find that it is converged at 0.5 (see appendix 4), so we have on average one superparticle for every two grid cells. This makes the computation affordable since the computational cost scales as  $N_p^2$ . Droplet growth by condensation is not incorporated in our model. We refer to Li et al. (2017) for a detailed description of our numerical setup and of the algorithm used to model collision.

The superparticle approach is computationally efficient (Li et al. 2017; Shima et al. 2009; Johansen et al. 2012), but it is an approximation. How accurately it describes the actual microscopic collision dynamics depends on several factors. In the limit where the number of droplets per superparticle tends to infinity, the algorithm reduces to a full mean-field description (Zsom and Dullemond 2008; Pruppacher et al. 1998). In the opposite limit, when the number of droplets per superparticle is small, the algorithm incorporates fluctuations in the collision processes that may be important in the dilute system that we consider here (Kostinski and Shaw 2005; Wilkinson 2016). Dziekan and Pawlowska (2017) compared the superparticle approach with the direct detection of collisions of point particles and concluded that the superparticle approach can accurately describes such fluctuations (Dziekan and Pawlowska 2017) as long as the number of droplet is less than 10 per superparticle. In our simulations, we assign two droplets per superparticle to ensure that the algorithm is sufficiently accurate.

In our simulations, we check for collisions at each time step, which enables us to get the size distribution  $f(r, t)$  at time  $t$ . Here  $r$  is the droplet radius. This distribution not only determines rain formation in clouds, but also the optical depth of the cloud (Beals et al. 2015). As initial condition, we adopt a log-normal droplet-size distribution (Seinfeld and Pandis 2016) since it can adequately model the droplet-size distribution function (e.g., in situ atmospheric measurements (Miles et al. 2000)),

$$f(r, 0) = \frac{n_0}{\sqrt{2\pi}\sigma_{\text{ini}} r} \exp\left[-\frac{\ln^2(r/r_{\text{ini}})}{2\sigma_{\text{ini}}^2}\right]. \quad (7)$$

Here  $r_{\text{ini}} = 10 \mu\text{m}$  and  $n_0 = n(t=0)$  is the initial number density of droplets. To speed up the computation by

a factor of a hundred, we adopt  $n_0 = 10^{10} \text{m}^{-3}$  instead of the typical value in the atmospheric clouds,  $10^8 \text{m}^{-3}$ ; cf. Li et al. (2017). We explore the convergence of  $\sigma_{\text{ini}}$  for collision driven by combined turbulence and gravity. It is found that  $\sigma_{\text{ini}}$  converges at 0.02 (see appendix 4). However, since gravity-generated collision is very sensitive to the initial size difference, we employ monodisperse initial distribution ( $\sigma_{\text{ini}} = 0$ ) for the case of combined turbulence and gravity. For turbulence-generated collision without gravity, we employ  $\sigma_{\text{ini}} = 0.2$ .

### 3. Results and discussion

#### a. Collision driven by turbulence

Figure 1(a) shows the time-averaged turbulent kinetic-energy spectra for different values of  $Re_\lambda$  at fixed  $\bar{\epsilon} \approx 0.04 \text{m}^2 \text{s}^{-3}$ . Here,  $Re_\lambda$  is varied by changing the domain size  $L$ , which in turn changes  $u_{\text{rms}}$ . For larger Reynolds numbers the spectra extend to smaller wavenumbers. Since the energy spectrum is compensated by  $\bar{\epsilon}^{-2/3} k^{5/3}$ , a flat profile corresponds to Kolmogorov scaling (Pope 2000). For the largest  $Re_\lambda$  in our simulations ( $Re_\lambda = 158$ ), the inertial range extends for about a decade in  $k$ -space. Figure 1(b) shows how the energy spectra depend on  $\bar{\epsilon}$ . Here we keep the values of  $Re_\lambda$  and  $\nu$  fixed, but vary  $u_{\text{rms}}$  by changing both  $L$  and the amplitude of the forcing; see Table 1 for details. Since the abscissa in the figures is normalized by  $k_\eta = 2\pi/\eta$ , the different spectra shown in Figure 1(b) collapse onto a single curve.

Figure 2(a) shows the droplet-size distributions obtained in our simulations for different values of  $Re_\lambda$ , but for the same  $\bar{\epsilon}$ . This figure demonstrates that the time evolution of the size distribution depends only weakly on  $Re_\lambda$  when  $\bar{\epsilon}$  is kept constant. This is consistent with the notion that the collisional growth is mainly dominated by the Kolmogorov scales (Saffman and Turner 1956; Devenish et al. 2012). The maximum Reynolds number in our DNS is  $Re_\lambda \approx 158$ . This value is still two orders of magnitude smaller than the typical value in atmospheric clouds (Grabowski and Wang 2013). It cannot be ruled out that there may be a stronger Reynolds-number effect on the collisional growth at higher Reynolds numbers (Shaw 2003; Ireland et al. 2016; Onishi and Seifert 2016). In the simulations of Onishi and Seifert (2016), where collisions are detected directly, the largest value of  $Re_\lambda$  was 333, which is twice as large as our largest value. They showed that the turbulence enhancement factor weakly depends on  $Re_\lambda$  when the mean radius of the initial distribution is  $10 \mu\text{m}$ . This is consistent with our results.

Figure 2(b) shows how the evolution of the droplet-size distribution depends on  $\bar{\epsilon}$ , for a fixed  $Re_\lambda$ . We see that especially the tails of the size distributions depend strongly on  $\bar{\epsilon}$ : the larger  $\bar{\epsilon}$ , the wider are the tails. The tails in the droplet-size distribution lead to a broad distribution of

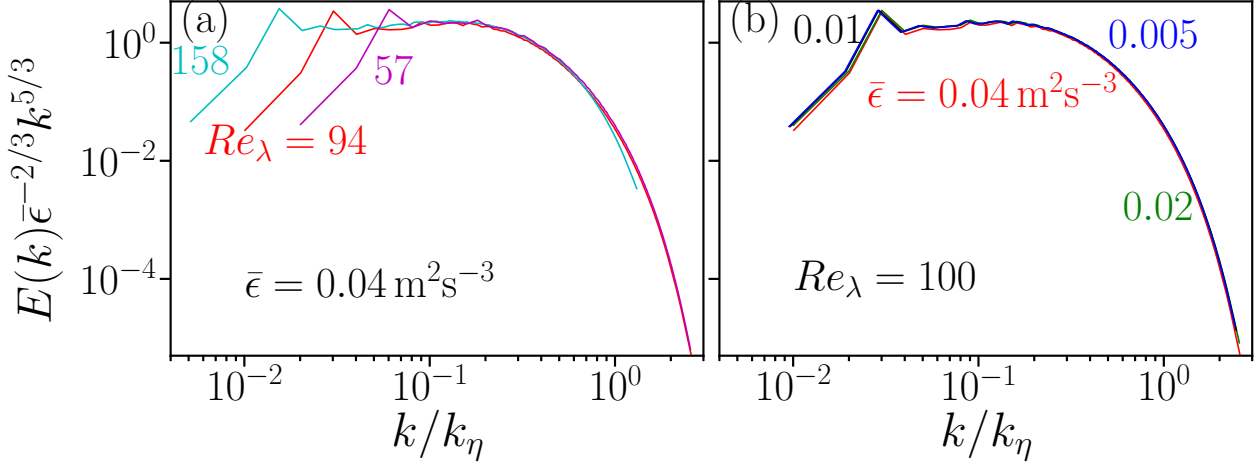


FIG. 1. Time-averaged kinetic energy spectra of the turbulence gas flow for (a) different  $Re_\lambda = 57$  (magenta dashed line), 94 (red solid line), and 158 (cyan dotted line) at fixed  $\bar{\epsilon} = 0.04 \text{ m}^2 \text{ s}^{-3}$  (see Runs A, B, and C in Table 1 for details) and for (b) different  $\bar{\epsilon} = 0.005 \text{ m}^2 \text{ s}^{-3}$  (blue dotted line), 0.01 (black dashed line), 0.02 (green dash-dotted line) and 0.04 (red solid line) at fixed  $Re_\lambda = 100$  (see Runs B, D, E, and F in Table 1 for details).

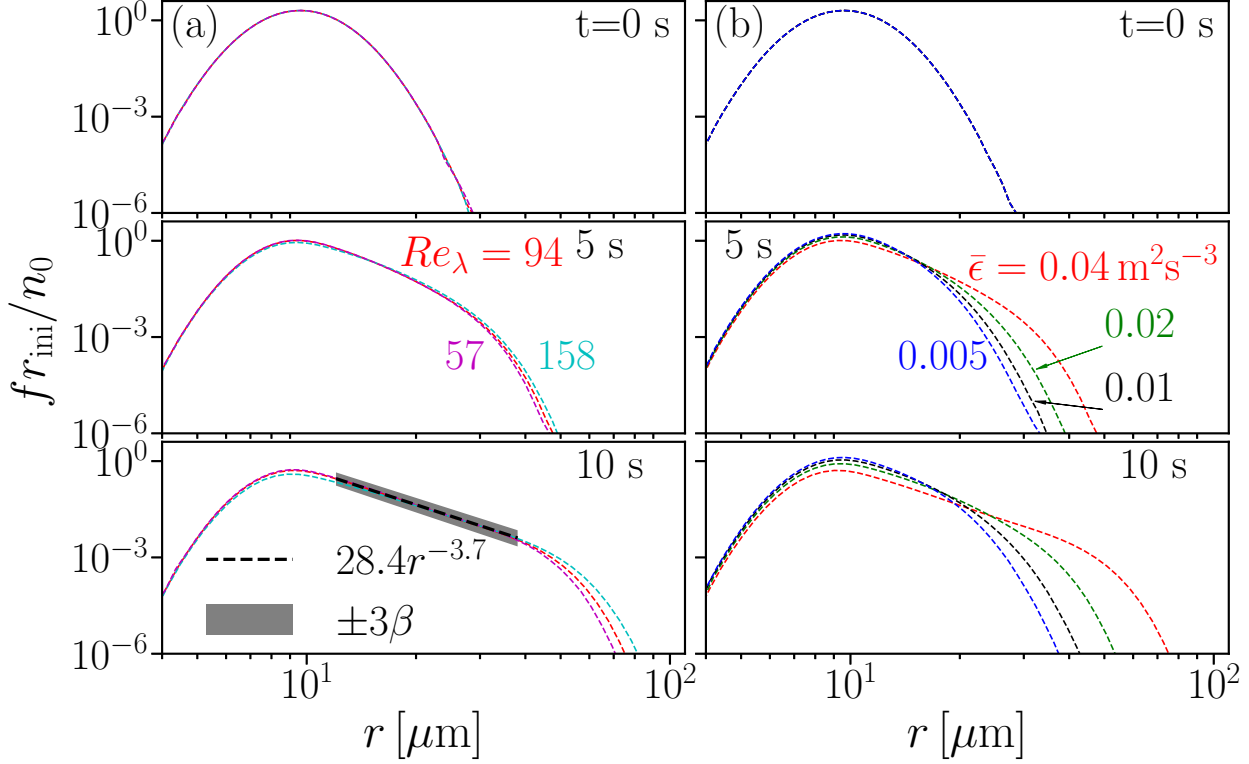


FIG. 2. Droplet-size distribution for the same simulations as in Figure 1. Panel (a): different  $Re_\lambda$  at fixed  $\bar{\epsilon}$ . Panel (b): different  $\bar{\epsilon}$  at fixed  $Re_\lambda$ . Here  $\beta$  is the standard deviation and  $3\beta$  is the significance level.

Stokes numbers. Also, since  $St = \tau_i / \tau_\eta \propto \bar{\epsilon}^{1/2}$ , the  $St$ -distribution shifts to large Stokes numbers as  $\bar{\epsilon}$  increases (see appendix 4).

We now show that the  $\bar{\epsilon}$ -dependence of the size distribution is due to the sensitive dependence of the collision rate upon this parameter. Figure 3 shows how the mean

collision rate  $\bar{R}_c$  changes as a function of time. This rate, which depends implicitly on  $\bar{\varepsilon}$ , is defined as

$$\bar{R}_c = \pi n_0 (2r)^2 \overline{|v|}, \quad (8)$$

where  $v$  is the relative velocity between two approaching droplets. This expression is written for identical droplets with radius  $r$ . In bidisperse suspensions with droplets of two different radii  $r_i$  and  $r_j$ ,  $2r$  is replaced by  $r_i + r_j$ . Collisions of small droplets advected by turbulence are due to local turbulent shear, provided that droplet inertia is negligible. Saffman and Turner (1956) proposed an expression for the resulting collision rate:

$$R_c^{S.T.} = \frac{C n_0 (2r)^3}{\tau_\eta}. \quad (9)$$

Saffman and Turner (1956) quote the value  $C = \sqrt{8\pi/15} \approx 1.29$  for the prefactor, but this is just an approximation, even at  $St = 0$  (Voßkuhle et al. 2014). It turns out that the Saffman-Turner estimate is an upper bound (Gustavsson and Mehlig 2016a), because it counts recollisions that must not be counted when the droplets coalesce upon collision, as in our simulations. Here recollision means that one droplet can experience several collision since there is no coalescence. DNS of small droplets in turbulence also count recollisions (no coalescence) and yield a value of  $C$  in good agreement with the Saffman-Turner estimate (Voßkuhle et al. 2014), in the limit of  $St \rightarrow 0$ .

In Figure 3(a) we normalized the mean collision rate by dividing with the Saffman-Turner expression (9) for the collision rate, averaging  $(2r)^3 = (r_i + r_j)^3$  over the initial size distribution. Initially the collision rate is of the same order as predicted by Eq. (9), but in our simulations the coefficient  $C$  depends on  $\varepsilon$ . It ranges from  $C \approx 1.57$  at  $\bar{\varepsilon} = 0.005 \text{ m}^2 \text{ s}^{-3}$  to  $C \approx 2.26$  at  $\bar{\varepsilon} = 0.04 \text{ m}^2 \text{ s}^{-3}$ . All values are somewhat larger than the Saffman-Turner prediction. This appears at variance with the expectation that the Saffman-Turner collision rate should be an upper bound for advected droplets. However, in our simulations the mean Stokes number ranges from  $St = 0.05$  for  $\bar{\varepsilon} = 0.005 \text{ m}^2 \text{ s}^{-3}$  to  $St = 0.14$  for  $\bar{\varepsilon} = 0.04 \text{ m}^2 \text{ s}^{-3}$ . From Figure 1 of Voßkuhle et al. (2014) we infer that  $C = 1.9$  for  $St = 0.05$ , in reasonable agreement with our simulation results. However, their  $C = 5$  for  $St = 0.14$ , which is about twice as large as our value ( $C \approx 2.26$ ). This overestimation of  $C$  at  $St = 0.14$  could be due to their recollisions. We conclude that the collision rate scales initially as predicted by the Saffman-Turner theory,  $R_c \sim \sqrt{\bar{\varepsilon}}$ , with small corrections due to particle inertia. At later times these corrections become larger. In recent years, several works have indicated that the Saffman-Turner model underestimates the collision rate at larger Stokes numbers when the effect of droplet inertia becomes important, so

that the droplets can detach from the flow. Model calculations show that this can substantially enhance the collision rate. Two mechanisms have been proposed.

First, droplet inertia causes identical droplets to cluster spatially (Maxey 1987; Elperin et al. 1996, 2002; Reade and Collins 2000; Kostinski and Shaw 2001; Bec 2003; Duncan et al. 2005; Elperin et al. 2013; Gustavsson and Mehlig 2016b). At small spatial scales the clustering of identical droplets is fractal. This enhances the collision rate of small droplets (Gustavsson et al. 2008a):  $R_c = C n_0 (2r)^3 \tau_\eta^{-1} g(2r)$ . Here  $g(2r)$  is the pair correlation function measuring the degree of fractal clustering of identical droplets:  $g(2r)$  diverges  $\sim r^{-\xi}$  as  $r \rightarrow 0$  with  $\xi > 0$ . The exponent  $\xi$  has been computed in DNS and model calculations (Gustavsson and Mehlig 2016b). It has a weak dependence on  $\bar{\varepsilon}$ . However,  $g(2r)$  is calculated based on the particle field with a single Stokes number, which makes it impossible to attempt a quantitative comparison between this theory and our simulation data. More importantly, collision leads to a distribution of droplet sizes. Droplets of different sizes cluster onto different fractal attractors. This may reduce the effect of spatial clustering on the collision rate (Chun et al. 2005; Bec et al. 2005; Meibohm et al. 2017).

Second, singularities in the droplet dynamics (so-called caustics) give rise to multi-valued droplet velocities, resulting in large velocity differences between nearby droplets (Sundaram and Collins 1997; Falkovich et al. 2002; Wilkinson et al. 2006; Falkovich and Pumir 2007; Gustavsson and Mehlig 2014; Voßkuhle et al. 2014). Most model calculations were performed for identical droplets. They indicate that the enhancement of the collision rate due to multi-valued droplet velocities dominates for Stokes numbers larger than unity (Voßkuhle et al. 2014). In this case, a Kolmogorov-scaling argument suggests (Mehlig et al. 2007; Gustavsson et al. 2008b) that  $R_c \sim n_0 r^2 u_K \sqrt{St} \propto \bar{\varepsilon}^{1/2}$ ; the  $\sqrt{St}$ -dependence was first suggested by Völk et al. (1980), using a different argument. This expression has the same  $\bar{\varepsilon}$ -dependence as Eq. (9). We note, however, that the Kolmogorov-scaling argument leading to this  $\sqrt{St}$ -dependence rests on the assumption that there is a well developed inertial range ( $Re_\lambda \rightarrow \infty$ ). This assumption is not fulfilled in our simulations. Moreover, at later times we expect that collisions between droplets of different sizes make an important contribution (Meibohm et al. 2017). Scaling theory (Mehlig et al. 2007) suggests that the  $\bar{\varepsilon}$ -scaling remains the same in the limit of  $Re_\lambda \rightarrow \infty$ . But, again, this limit is not realized in our simulations. Also, any theory for the collision rate in bidisperse suspensions must be averaged over the distribution of particle sizes and their velocities to allow comparison with Figure 3(a). This may introduce additional  $\bar{\varepsilon}$ -dependencies. It is therefore plausible that the small- $St$  scaling,  $R_c \sim \sqrt{\bar{\varepsilon}}$ , breaks down in our simulations at larger Stokes numbers, indicating

that the increase in the mean collision rate is an inertial effect. Moreover, since the Stokes numbers are larger for larger values of  $\bar{\epsilon}$ , we expect the inertial additive corrections to the collision rate (due to clustering and increased relative particle velocities) to be larger at larger  $\bar{\epsilon}$ . This is consistent with Figure 3(a). In conclusion, the mean collision rate depends strongly on  $\bar{\epsilon}$  (Figure 3(a)), as do the size distributions shown in Figure 2(b).

Figure 3(b) shows that the mean collision rate depends only weakly on the Reynolds number. It demonstrates that the collision rate is somewhat larger for larger Reynolds numbers. This is consistent with the notion that particle pairs exploring the inertial range collide at larger relative velocities when the inertial range is larger (Gustavsson et al. 2008b). But, as pointed out above, the inertial range in our simulations is too small for this mechanism to have a substantial effect.

It is interesting to note that the size distribution exhibits power law distribution in the range of  $10 \sim 40 \mu\text{m}$ , as shown in the third panel of Figure 2(a). A slope of  $-3.7$  is observed. The observed size distribution of interstellar dust grains shows power law distribution with a slope  $-3.3 \sim -3.6$  (Mathis et al. 1977). The collisional growth of dust grains in a intensive turbulent environment is one of the main mechanisms for planet formation (Johansen and Lambrechts 2017). Another example of the observed power law size distribution is the size distribution of particles in Saturn's rings (Brilliantov et al. 2015), where a slope of  $-3$  is observed. This power law size distribution may be universal for turbulence-generated collisional growth.

#### b. Collision driven by combined turbulence and gravity

For cloud-droplet growth, gravitational settling is significant (Woittiez et al. 2009; Grabowski and Wang 2013). Collision driven by gravity is very sensitive to the initial size difference (see appendix 4). To avoid any bias from the initial size difference, we adopt a monodisperse initial distribution, i.e.,  $\sigma_{\text{ini}} = 0$ . In Figure 4, we compare the evolution of the droplet-size distribution for the turbulent case and the combined case with turbulence and gravity. At  $t = 1$  s, both cases have almost the same droplet-size distribution, demonstrating that turbulence dominates the collisional growth. When  $t \geq 1$  s, gravity dominates the time evolution of the droplet-size distribution. The tail of the droplet-size distribution reaches  $80 \mu\text{m}$  (drizzle-size) for the combined turbulence and gravity case at  $t = 9$  s. For the turbulence case, the tail reaches  $48 \mu\text{m}$  after the same time, which is roughly half the radius obtained for the combined turbulence and gravity case. Since our initial number density of cloud droplets is a hundred times larger than the typical value in atmospheric clouds, we can scale our simulation time by a factor of a hundred. Thus, a scaled time of 9 s, for example, corresponds to 900 s

in atmospheric clouds. We find that collisional growth of cloud droplets can reach drizzle-sized droplets in about 900 s = 15 min. This time scale is comparable to the time scale for rapid warm rain formation.

Next, we check the  $\bar{\epsilon}$  dependency for the combined turbulence & gravity case. As shown in Figure 5, the collisional growth depends on  $\bar{\epsilon}$ , but the dependency is weaker than the case without gravity, as can be seen from Figure 2(b). When gravity is included, the non-dimensional terminal velocity  $Sv = v_g/u_\eta$ , characterizing the relative droplet inertia and gravitational sedimentation, becomes important (Devenish et al. 2012) (Here we adopt  $Sv$  because it contains the information of particle size compared with the Froude number of particles defined as  $Fr = |g|\tau_\eta/u_\eta$  (Gustavsson et al. 2014)).  $Sv$  can be expressed as  $Sv = FrSt$ , where  $v_g = \tau_i g$  is the terminal fall velocity and  $u_\eta$  is the turbulent velocity at the Kolmogorov scale  $\eta$ . It can also be interpreted as the ratio of the Kolmogorov eddy turnover time and the time it takes for a particle to sediment across the eddy. If the ratio is much larger than unity, the particle will rapidly sediment through the eddy, thereby leading to weak particle-eddy interaction. On the other hand, if  $Sv$  is much smaller than unity, sedimentation does not play a significant role in reducing the time of particle-eddy interaction (Ayala et al. 2008). The distribution of  $Sv$  also shows only a weak dependency on  $\bar{\epsilon}$  in our simulations as demonstrated in Figure 5.

Further inspection of the mean collision rate  $\bar{R}_c$  (Figure 6) is consistent with the above observations. More importantly, the normalized  $\bar{R}_c$  collapse onto each other and follow exponential growth. This can be explained by the following theory of the continuous collision (Lamb and Verlinde 2011). Given two droplets of very different sizes that collide with each other due to gravity, the collision rate given by equation (6) is

$$\bar{R}_c^{\text{continuous}} = \pi(r_L + r_S)^2 |V_L - V_S|. \quad (10)$$

When  $Re_\lambda$  is large and  $r_L \gg r_S$ , equation (5) yields  $V_L \propto r_L^{0.78}$ . The linear approximation for the velocity (Lamb and Verlinde 2011) is now obtained by replacing the exponent 0.78 with unity, such that equation (10) simplifies to

$$\bar{R}_c^{\text{continuous}} \sim r_L^3. \quad (11)$$

The rate of mass increase,  $dm_L/dt$ , is proportional to the collision rate. Therefore, equation (11) can also be expressed as

$$\frac{dm_L}{dt} \sim r_L^3. \quad (12)$$

Combine equations (11) and (12), we can obtain the exponential growth of  $\bar{R}_c$ ,

$$\bar{R}_c^{\text{continuous}} \sim \exp(\alpha t), \quad (13)$$

where  $\alpha$  is a constant.

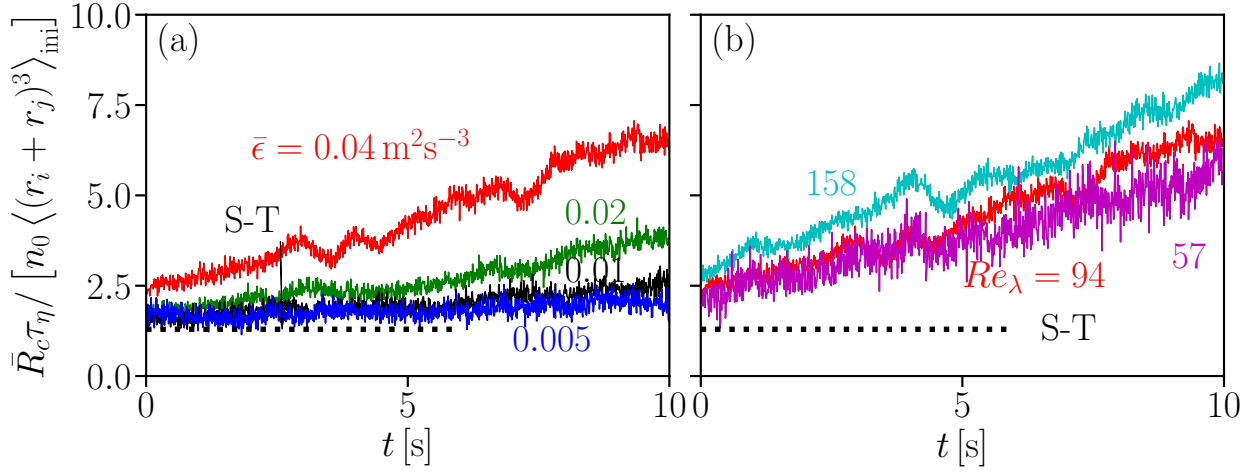


FIG. 3. Mean collision rate for same simulations as in Figure 1. Panel (a): different  $\bar{\epsilon}$  at fixed  $Re_\lambda$ . Panel (b): different  $Re_\lambda$  at fixed  $\bar{\epsilon}$ . In both panels the data are normalized by dividing by  $n_0 \langle (r_i + r_j)^3 \rangle_{\text{ini}} / \tau_\eta$ .

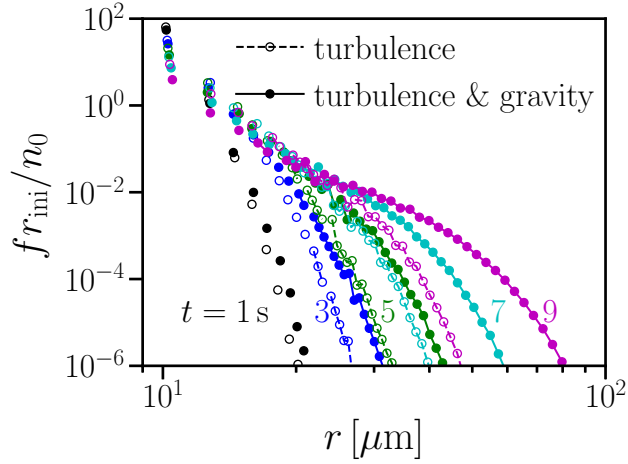


FIG. 4. Time evolution of the droplet-size distribution. Comparing pure turbulence case (open symbols) with turbulence & gravity case (filled symbols). The time interval is 2 s, plotted from 1 s to 9 s (from left to right). The mean energy dissipation rate is  $\bar{\epsilon} = 0.04 \text{ m}^2 \text{ s}^{-3}$  and  $Re_\lambda = 100$ . The droplets are all of size  $10 \mu\text{m}$  initially; see Run D in Table 1 for details of the simulation.

The excellent agreement between our simulation and the theory demonstrates that the continuous growth theory is robust. Even in the circumstance that we detect the collision rate directly by counting each collision event without any assumptions, such as that of large size differences, the linear approximation for the velocity Lamb and Verlinde (2011), and the absence of turbulence. When  $\bar{R}_c$  is normalized by  $\tau_\eta$ , the curves representing different  $\bar{\epsilon}$  collapses onto each other. This indicates that (1) gravity dominates the collisional growth; (2) collision time scale is smaller than the Kolmogorov time scale; (3) turbulence is respon-

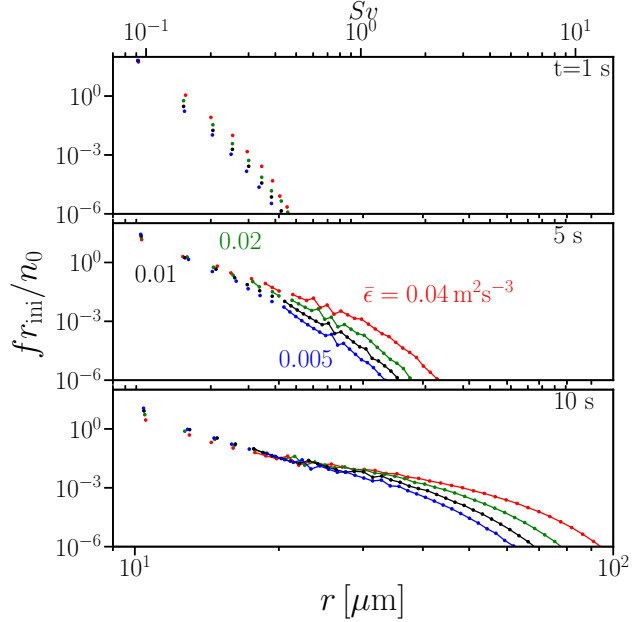


FIG. 5. Time evolution of the droplet-size distribution for different  $\bar{\epsilon}$  in combined turbulence & gravity environment.  $Re_\lambda = 100$ . Droplets are all with size  $10 \mu\text{m}$  initially. See Runs A, B, C, and D in Table 1 for details of the simulations.

sible for generating few larger droplets so that the gravitational collision can be triggered at the initial phase of rain-drop formation; (4) turbulence transport provides a mean effect for collision as implicitly indicated in equation (9).

In the atmospheric clouds, the size distribution of cloud droplets has a certain width. To investigate the collisional growth with a lognormal initial distribution when there



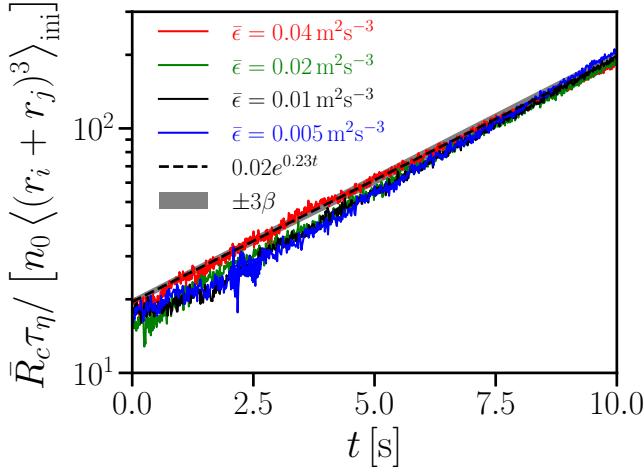


FIG. 6. Mean collision rate  $\bar{R}_c$  for different  $\bar{\epsilon}$ . Same simulations as in Figure 5. Here  $\beta$  is the standard deviation and  $3\beta$  is the significance level.

is both turbulence and gravity, we use the same setup as in Figure 2(b), but with gravity included. As shown in Figure 7(a), the evolution of the droplet-size distribution depends only weakly on the energy dissipation rate. This again confirms the notion that gravity-generated collision is very sensitive to the initial size difference. To further illustrate this, we plot the time evolution of the size distribution with different initial widths, as shown in Figure 7(b). We also compare the present numerical simulations with the idealized gravity-driven collision. As shown by the brown dashed lines in Figure 7(a), turbulence does not enhance the collisional growth strongly. The mass distribution function is another quantity to characterize different growth phases of cloud droplets (Berry and Reinhardt 1974). Similar to the size distribution, the effect of turbulence on different growth phases of cloud droplets is weak (see appendix 4) in our simulations.

#### 4. Conclusions

In the present study we have addressed the problem of turbulence effects on collisional growth of particles such as cloud droplets. We have investigated this effect using a superparticle approximation for the droplet dynamics in combination with high-resolution DNS of fully-developed turbulence. In the absence of gravity, we found that the droplet-size distribution depends sensitively on the mean energy-dissipation rate  $\bar{\epsilon}$  at fixed  $\text{Re}_\lambda$ , which we related to the  $\bar{\epsilon}$ -dependence of the mean collision rate. We found that this rate increases as  $\bar{\epsilon}^{1/2}$  (except for the largest values of  $\bar{\epsilon}$  simulated). This is consistent with the Saffman-Turner collision model and its extensions. A more detailed comparison with these calculations is not possible

at this point, because there is no prediction for the prefactors in general. The size distribution due to turbulence-generated collisions exhibits power law behavior with a slope of  $-3.7$  in the size range of about  $10 \sim 40 \mu\text{m}$ , which is close to the power law size distribution of interstellar dust grains. This indicates that the power law size distribution may be universal (Mathis et al. 1977). When gravity is invoked, the strong dependency on the mean energy dissipation rate weakens.

When collisions are driven by both turbulence and gravity, we found that turbulence is crucial for driving the collision so that a few large cloud droplets can be formed in the initial stage of raindrop formation. Gravity takes over as the main driver for droplet collisions when the radius of cloud droplets reaches the size of about  $20 \mu\text{m}$ . With combined turbulence and gravity, the time scale for reaching drizzle-sized droplets is about 900 s, which is close to the time scale of the rapid warm rain formation. The collision rate grows exponentially, which is consistent with the theoretical prediction of the continuous growth even when turbulence is invoked. The theory of continuous collisions is built upon the assumptions of huge size differences, a linear drag force, and gravity-driven collisions. These assumptions are not applicable to the present simulations. The consistency between our simulations and the theory suggests that the theory is remarkably robust. This also indicates that (1) gravity dominates the collisional growth; (2) the collision time scale is smaller than the Kolmogorov time scale; (3) turbulence is responsible for generating a few larger droplets so that gravitational collisions can occur at the initial phase of raindrop formation; (4) turbulence transport provides a mean effect for collisions, as implied by equation (9).

Collisional growth of cloud droplets due to turbulence and gravity is very sensitive to the tail of the initial size distribution. As already discussed previously (Li et al. 2017), this problem is being alleviated by considering the combined condensational and collisional growth. Especially the condensational growth due to supersaturation fluctuations may result in larger tails of the size distribution (Sardina et al. 2015; Chandrakar et al. 2016). This is another subject of an ongoing separate study.

**Acknowledgments.** We thank Akshay Bhatnagar and Gregory Falkovich for stimulating discussions. This work was supported through the FRINATEK grant 231444 under the Research Council of Norway, SeRC, the Swedish Research Council grants 2012-5797 and 2013-03992, and the grant “Bottlenecks for particle growth in turbulent aerosols” from the Knut and Alice Wallenberg Foundation, Dnr. KAW 2014.0048. Gunilla Svensson also thanks the Wenner-Gren Foundation for their support.” The simulations were performed using resources provided by the Swedish National Infrastructure for Computing (SNIC) at the Royal Institute

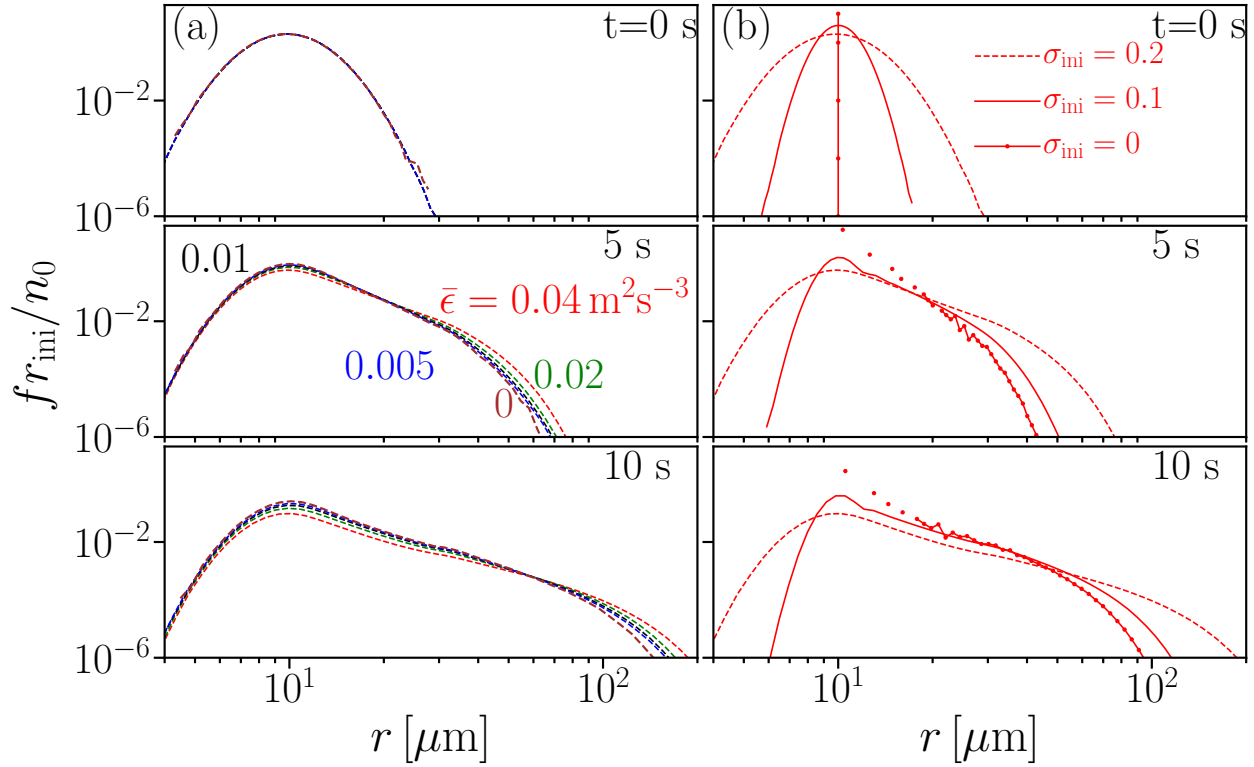


FIG. 7. Same simulations as in Figure 2 but with gravity invoked. (a): time evolution of size distribution for different  $\bar{\epsilon}$  with  $\sigma_{\text{ini}} = 0.2$ ; the brown dashed lines represent the size distribution due to gravity-generated collision. (b): comparison among  $\sigma_{\text{ini}} = 0, 0.1$ , and  $0.2$  with  $\bar{\epsilon} = 0.04 \text{ m}^2 \text{ s}^{-3}$ .

of Technology in Stockholm and Chalmers Centre for Computational Science and Engineering (C3SE). This work also benefited from computer resources made available through the Norwegian NOTUR program, under award NN9405K. The source code used for the simulations of this study, the PENCIL CODE, is freely available on <https://github.com/pencil-code/>. The input files as well as some of the output files of the simulations listed in Table 1 are available under <http://www.nordita.org/~brandenb/projects/collision-turbulence/>.

## APPENDIX A

### Effect of initial condition on collision in a turbulent environment

The initial conditions are important for the collision. We tested three different initial conditions. Collision is triggered (1) in a randomly distributed superparticle field and the velocity of the flow is zero, (2) in a well-mixed particle field and the velocity of the flow is zero, and (3) in a well-mixed particle field and the turbulence is well-developed. To compare the time evolution of the size distribution for these three cases, we first define the normal-

ized moments of the size distribution (Li et al. 2017),

$$a_\zeta = \left( \int_0^\infty f r^\zeta dr / \int_0^\infty f dr \right)^{1/\zeta} \quad (\text{A1})$$

where  $\zeta$  is a positive integer. The mean radius  $\bar{r}$  is given by  $a_1$ , the maximum radius is  $\max(r) = a_\infty$ , and the droplet mass is proportional to the third power of  $a_3$ .  $a_\zeta$  can characterize the size distribution with simpler diagnostics. Figure A8 shows  $a_\zeta$  for the three different initial conditions. It is obvious that the time evolution of  $a_\zeta$  is independent from initial conditions. This can sufficiently save computational time.

## APPENDIX B

### Statistical convergence of the number of superparticles per grid cell in a turbulent environment

As discussed in Section 2, simulations with massive number of superparticles is computationally costing. In Li et al. (2017), we found that the initial  $N_p/N_{\text{grid}}$  converges at 4 when the collision is driven by gravity without turbulence. In the present study,  $N_{\text{grid}} = 512^3$ .  $N_p/N_{\text{grid}} = 4$  will result in  $N_p = 4 \times 512^3 = 536870912$ , which will be

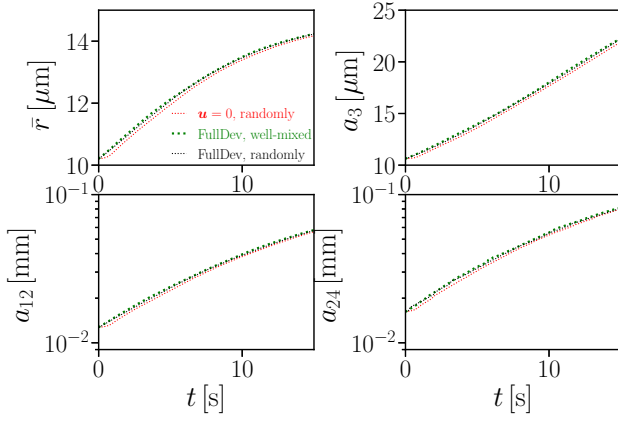


FIG. A8. Comparison of  $a_z$  for different initial conditions: collision is triggered (1) (red curve) in a randomly distributed superparticle field and the velocity of the flow is zero, (2) (black curve) in a well-mixed particle field and the velocity of the flow is zero, and (3) (green curve) in a well-mixed particle field and the turbulence is well-developed. Gravity is omitted here.  $L = 0.25$  m. The initial size distribution is given by equation (7) with  $r_{\text{ini}} = 10 \mu\text{m}$  and  $\sigma_{\text{ini}} = 0.2$ . The number of mesh grid points is  $128^3$ .  $f_0 = 0.02$ .  $N_p/10^6 = 8.4$ . These result in  $\text{Re}_\lambda = 100$  and  $\bar{\epsilon} = 0.03 \text{ m}^2 \text{ s}^{-3}$ .

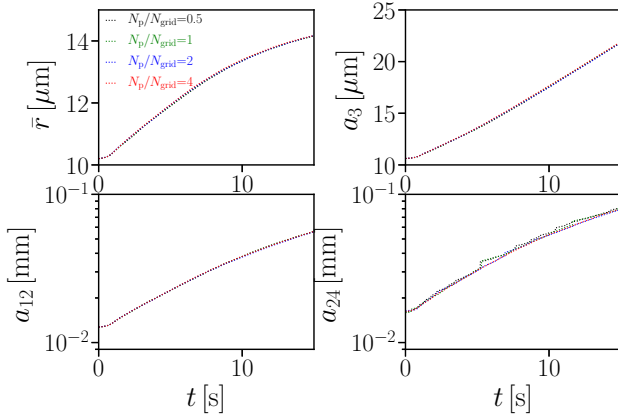


FIG. B9. Comparison of  $a_z$  for different  $N_p/N_{\text{grid}}$ . Here  $N_{\text{grid}} = 128^3$  is fixed.  $N_p/N_{\text{grid}}$  even converges at 0.5. Same simulations as in Figure A8 but with different  $N_p$ .

very computationally demanding. This motivates us to re-study the convergence of  $N_p/N_{\text{grid}}$  in high Reynolds number turbulence case instead of carrying the convergence study from pure gravity case to the turbulence case. As shown in Figure B9,  $N_p/N_{\text{grid}}$  converges at 0.5. This could be due to the fact that turbulence transports particles sufficiently.

## APPENDIX C

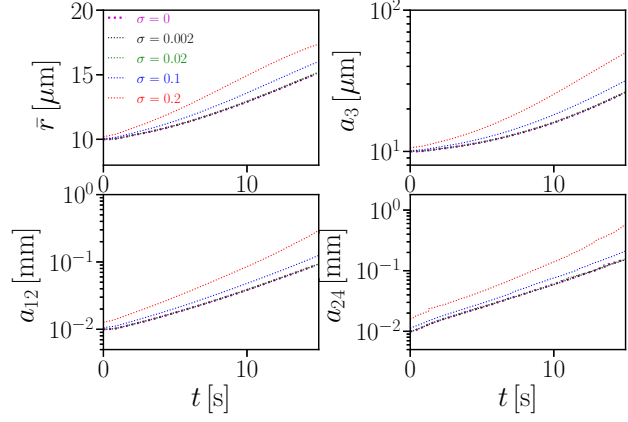


FIG. C10. Convergence of  $\sigma_{\text{ini}}$ . Collision is driven by combined turbulence and gravity; see Run B for simulation details.

## Convergence of the initial width $\sigma_{\text{ini}}$ in a turbulent environment with gravity

Since the gravity-driven collision is sensitive to the size difference, we investigated the convergence of the width  $\sigma_{\text{ini}}$  in equation (7) in a combined turbulence and gravity environment. Figure C10 shows that  $\sigma_{\text{ini}}$  converges at 0.02. However, as we have discussed in Section b, we choose  $\sigma_{\text{ini}} = 0$  for the combined turbulence and gravity case.

## APPENDIX D

### Distribution of the Stokes number

Figure D11 shows the distribution function of Stokes numbers for the same simulations as in Figure 2. Initially, the distribution of Stokes number shifts to the right with increasing  $\bar{\epsilon}$ , which will trigger stronger collisional growth. At later times, when  $\bar{\epsilon}$  increases from  $0.005$  to  $0.04 \text{ m}^2 \text{ s}^{-3}$ , the tail of the Stokes number distribution increases by more than an order of magnitude, which leads to an extension of about three orders of magnitude at  $t = 10$  s. This indicates that the collisional growth rate strongly depends on the Stokes number. Increasing  $\bar{\epsilon}$  results in a larger range of variations in the value of the Stokes number, thus enhancing the collisional growth.

## APPENDIX E

### Mass distribution function

Berry and Reinhardt (1974) developed a model to describe the growth process of cloud droplets. We use the same nomenclature of the mass distribution as Berry and Reinhardt (1974),  $g(\ln r, t)$ . The mean

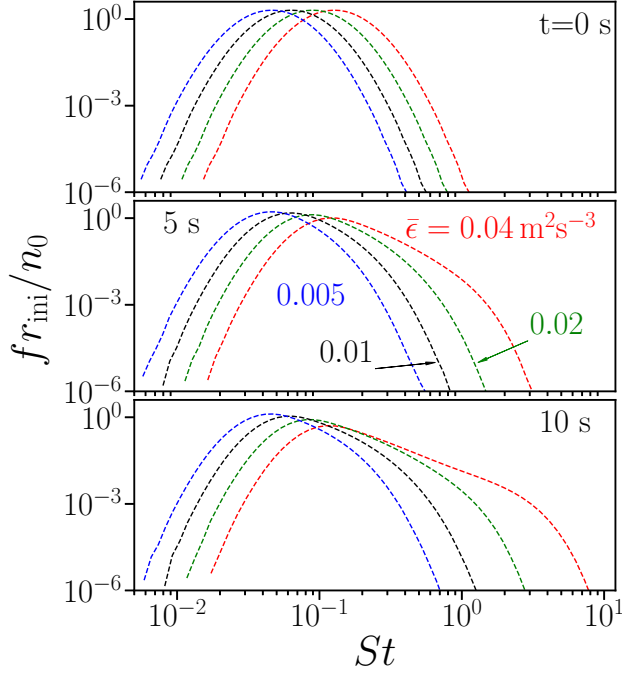


FIG. D11. Time evolution of the Stokes number distribution  $St(r,t)$  for different  $\bar{\epsilon}$  with fixed  $Re_\lambda$ . Same simulations as in Figure 2.

mass of liquid water in terms of the size distribution function  $f(r,t)$  is  $\bar{M} = \frac{4}{3}\pi\rho \int_0^\infty f(r,t)dr$ , which is  $\bar{M} = \int_0^\infty g(\ln r,t)d\ln r$  in terms of  $g(\ln r,t)$ . Therefore,  $g(\ln r,t) = (4\pi/3)\rho r^4 f(r,t)$ . Figure E12 shows  $g(\ln r,t)$  calculated from the same simulations as in Figure 7, where the collision is driven by both gravity and turbulence.  $g(\ln r,t)$  shows noticeable dependency on  $\bar{\epsilon}$ . The broadening of  $g(\ln r,t)$  is due to the auto-conversion as described by Berry and Reinhardt (1974). The auto-conversion phase is characterized by the primary peak, where droplets with similar size collide and merge to larger droplets. The formation of the larger droplets leads to the second phase, accretion, which is characterized by the second peak. In this phase, larger droplets sweep the smaller ones near the primary peak. Therefore, the second peak occurs. Turbulence indeed enhances these phases. However, the enhancement is weak.

## References

Andersson, B., K. Gustavsson, B. Mehlig, and M. Wilkinson, 2007: Advective collisions. *Europhys. Lett.*, **80** (6), 69001.

Ayala, O., B. Rosa, L.-P. Wang, and W. W. Grabowski, 2008: Effects of turbulence on the geometric collision rate of sedimenting droplets. part 1. results from direct numerical simulation. *New J. Phys.*, **10** (7), 075015.

Beals, M. J., J. P. Fugal, R. A. Shaw, J. Lu, S. M. Spuler, and J. L. Stith, 2015: Holographic measurements of inhomogeneous

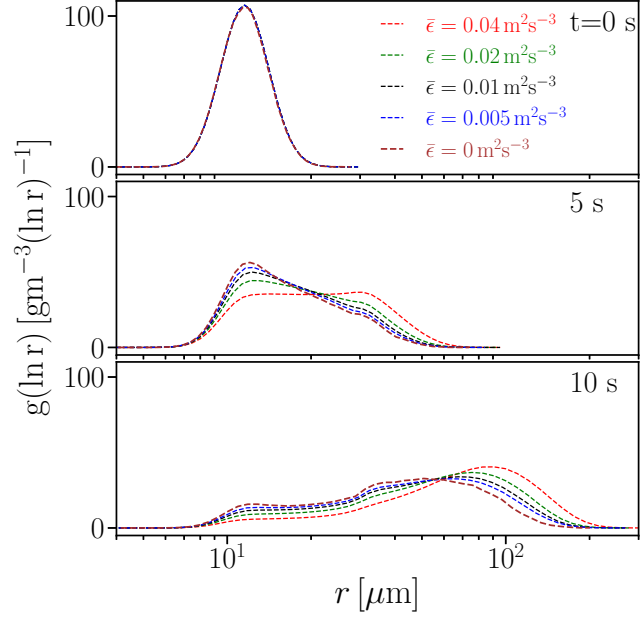


FIG. E12. Time evolution of the mass distribution function  $g(\ln r; t)$ . Same simulations as in Figure 7(a).

cloud mixing at the centimeter scale. *Science*, **350** (6256), 87–90, <http://science.sciencemag.org/content/350/6256/87.full.pdf>.

Bec, J., 2003: Fractal clustering of inertial particles in random flows. **15**, 81–84.

Bec, J., A. Celani, M. Cencini, and S. Musacchio, 2005: Clustering and collisions in random flows. **17**, 073301.

Berry, E. X., and R. L. Reinhardt, 1974: An analysis of cloud drop growth by collection: Part i. double distributions. *Journal of the Atmospheric Sciences*, **31** (7), 1814–1824.

Brandenburg, A., 2001: The inverse cascade and nonlinear alpha-effect in simulations of isotropic helical hydromagnetic turbulence. *Astro-phys. J.*, **550** (2), 824.

Brilliantov, N., P. Krapivsky, A. Bodrova, F. Spahn, H. Hayakawa, V. Stadnichuk, and J. Schmidt, 2015: Size distribution of particles in saturns rings from aggregation and fragmentation. *Proceedings of the National Academy of Sciences*, **112** (31), 9536–9541.

Chandrakar, K. K., W. Cantrell, K. Chang, D. Ciochetto, D. Niedermeier, M. Ovchinnikov, R. A. Shaw, and F. Yang, 2016: Aerosol indirect effect from turbulence-induced broadening of cloud-droplet size distributions. *Proc. Nat. Acad. Sci.*, **113** (50), 14 243–14 248.

Chun, J., D. L. Koch, S. L. Rani, A. Ahluwalia, and L. R. Collins, 2005: Clustering of aerosol particles in isotropic turbulence. **536**, 219–251.

Devenish, B., and Coauthors, 2012: Droplet growth in warm turbulent clouds. *Quart. J. Roy. Meteorol. Soc.*, **138** (667), 1401–1429.

Duncan, K., B. Mehlig, S. Östlund, and M. Wilkinson, 2005: Clustering in mixing flows. **95**, 240602.

- Dziekan, P., and H. Pawlowska, 2017: Stochastic coalescence in lagrangian cloud microphysics. *Atmosph. Chemistry and Physics*, **2017**, 1–18.
- Elperin, T., N. Kleeorin, M. Liberman, and I. Rogachevskii, 2013: Tangling clustering instability for small particles in temperature stratified turbulence. *Phys. Fluids*, **25** (8), 085 104.
- Elperin, T., N. Kleeorin, V. S. L'vov, I. Rogachevskii, and D. Sokoloff, 2002: Clustering instability of the spatial distribution of inertial particles in turbulent flows. *Phys. Rev. E*, **66**, 036 302.
- Elperin, T., N. Kleeorin, and I. Rogachevskii, 1996: Self-excitation of fluctuations of inertial particle concentration in turbulent fluid flow. *Phys. Rev. Lett.*, **77**, 5373–5376.
- Falkovich, G., A. Fouxon, and M. Stepanov, 2002: Acceleration of rain initiation by cloud turbulence. *Nature*, **419** (6903), 151–154.
- Falkovich, G., and A. Pumir, 2007: Sling effect in collisions of water droplets in turbulent clouds. *J. Atmosph. Sci.*, **64** (12), 4497–4505.
- Grabowski, W. W., and L.-P. Wang, 2013: Growth of cloud droplets in a turbulent environment. *Annu. Rev. Fluid Mech.*, **45** (1), 293–324, <http://dx.doi.org/10.1146/annurev-fluid-011212-140750>.
- Gustavsson, K., and B. Mehlig, 2014: Relative velocities of inertial particles in turbulent aerosols. *J. Turbulence*, **15** (1), 34–69, <http://dx.doi.org/10.1080/14685248.2013.875188>.
- Gustavsson, K., and B. Mehlig, 2016a: Statistical model for collisions and recollisions of inertial particles in mixing flows. *The European Physical Journal E*, **39** (5), 55.
- Gustavsson, K., and B. Mehlig, 2016b: Statistical models for spatial patterns of heavy particles in turbulence. *Advances in Physics*, **65** (1), 1–57, <http://dx.doi.org/10.1080/00018732.2016.1164490>.
- Gustavsson, K., B. Mehlig, and M. Wilkinson, 2008a: Collisions of particles advected in random flows. *New J. Phys.*, **10** (7), 075 014.
- Gustavsson, K., B. Mehlig, M. Wilkinson, and V. Uski, 2008b: Variable-range projection model for turbulence-driven collisions. **101**, 174503.
- Gustavsson, K., S. Vajedi, and B. Mehlig, 2014: Clustering of particles falling in a turbulent flow. *Phys. Rev. Lett.*, **112**, 214 501.
- Ireland, P. J., A. D. Bragg, and L. R. Collins, 2016: The effect of reynolds number on inertial particle dynamics in isotropic turbulence. part 1. simulations without gravitational effects. *J. Fluid Mech.*, **796**, 617–658.
- Johansen, A., and M. Lambrechts, 2017: Forming planets via pebble accretion. *Annual Review of Earth and Planetary Sciences*, **45**, 359–387.
- Johansen, A., A. N. Youdin, and Y. Lithwick, 2012: Adding particle collisions to the formation of asteroids and kuiper belt objects via streaming instabilities. *Astron. Astroph.*, **537**, A125.
- Kostinski, A. B., and R. A. Shaw, 2001: Scale-dependent droplet clustering in turbulent clouds. *J. Fluid Mech.*, **434**, 389–398.
- Kostinski, A. B., and R. A. Shaw, 2005: Fluctuations and luck in droplet growth by coalescence. *Bull. Am. Met. Soc.*, **86**, 235–244.
- Lamb, D., and J. Verlinde, 2011: *Physics and Chemistry of Clouds*, chap. 11, 438. Cambridge, England, Cambridge Univ. Press.
- Li, X.-Y., A. Brandenburg, N. E. L. Haugen, and G. Svensson, 2017: Eulerian and lagrangian approaches to multidimensional condensation and collection. *J. Advances Model. Earth Systems*, **9**, 1116–1137.
- Marchioli, C., and Coauthors, 2008: Statistics of particle dispersion in direct numerical simulations of wall-bounded turbulence: Results of an international collaborative benchmark test. *Intern. J. Multiphase Flow*, **34** (9), 879–893.
- Mathis, J. S., W. Rumpl, and K. H. Nordsieck, 1977: The size distribution of interstellar grains. *The Astrophysical Journal*, **217**, 425–433.
- Maxey, M., 1987: The gravitational settling of aerosol particles in homogeneous turbulence and random flow fields. *J. Fluid Mech.*, **174**, 441–465.
- Mehlig, B., M. Wilkinson, and V. Uski, 2007: Colliding particles in highly turbulent flows. *Phys. Fluids*, **19**, 098107.
- Meibohm, J., L. Pistone, K. Gustavsson, and B. Mehlig, 2017: Relative velocities in bidisperse turbulent suspensions. *e-preprint, arXiv:1703.01669*.
- Miles, N. L., J. Verlinde, and E. E. Clothiaux, 2000: Cloud droplet size distributions in low-level stratiform clouds. *Journal of the atmospheric sciences*, **57** (2), 295–311.
- Onishi, R., and A. Seifert, 2016: Reynolds-number dependence of turbulence enhancement on collision growth. *Atmosph. Chemistry and Physics*, **16** (19), 12 441–12 455.
- Pope, S., 2000: *Turbulent Flows*. Cambridge University Press.
- Pruppacher, H. R., J. D. Klett, and P. K. Wang, 1998: *Microphysics of clouds and precipitation*. Taylor & Francis.
- Pumir, A., and M. Wilkinson, 2016: Collisional aggregation due to turbulence. *Annual Review of Condensed Matter Physics*, **7**, 141–170.
- Reade, W. C., and L. R. Collins, 2000: Effect of preferential concentration on turbulent collision rates. *Phys. Fluids*, **12** (10), 2530–2540.
- Saffman, P. G., and J. S. Turner, 1956: On the collision of drops in turbulent clouds. *J. Fluid Mech.*, **1**, 16–30.
- Saito, I., and T. Gotoh, 2017: Turbulence and cloud droplets in cumulus clouds. *New Journal of Physics*.
- Sardina, G., F. Picano, L. Brandt, and R. Caballero, 2015: Continuous growth of droplet size variance due to condensation in turbulent clouds. *Phys. Rev. Lett.*, **115** (18), 184 501.
- Schiller, L., and A. Naumann, 1933: Fundamental calculations in gravitational processing. *Zeitschrift Des Vereines Deutscher Ingenieure*, **77**, 318–320.
- Seinfeld, J. H., and S. N. Pandis, 2016: *Atmospheric chemistry and physics: from air pollution to climate change*. John Wiley & Sons.
- Shaw, R. A., 2003: Particle-turbulence interactions in atmospheric clouds. *Annu. Rev. Fluid Mech.*, **35** (1), 183–227.
- Shima, S., K. Kusano, A. Kawano, T. Sugiyama, and S. Kawahara, 2009: The super-droplet method for the numerical simulation of clouds and precipitation: a particle-based and probabilistic microphysics model coupled with a non-hydrostatic model. *Quart. J. Roy. Met. Soc.*, **135**, 1307–1320, physics/0701103.

- Sundaram, S., and L. R. Collins, 1997: Collision statistics in an isotropic particle-laden turbulent suspension. *J. Fluid. Mech.*, **335**, 75–109.
- Veysey, J., II, and N. Goldenfeld, 2007: Simple viscous flows: From boundary layers to the renormalization group. *Reviews of Modern Physics*, **79** (3), 883–927.
- Völk, H. J., F. C. Jones, G. E. Morfill, and S. Röser, 1980: Collisions between grains in a turbulent gas. *A & A*, **85**, 316.
- Voßkuhle, M., A. Pumir, E. Lévéque, and M. Wilkinson, 2014: Prevalence of the sling effect for enhancing collision rates in turbulent suspensions. *J. Fluid Mech.*, **749**, 841–852.
- Wang, L.-P., and W. W. Grabowski, 2009: The role of air turbulence in warm rain initiation. *Atmosph. Sci. Lett.*, **10** (1), 1–8.
- Wang, L.-P., A. S. Wexler, and Y. Zhou, 1998: Statistical mechanical descriptions of turbulent coagulation. *Physics of Fluids*, **10** (10), 2647–2651.
- Wilkinson, M., 2016: Large deviation analysis of rapid onset of rain showers. *Phys. Rev. Lett.*, **116** (1), 018 501.
- Wilkinson, M., B. Mehlig, and V. Bezuglyy, 2006: Caustic activation of rain showers. *Phys. Rev. Lett.*, **97**, 048 501.
- Woittiez, E. J. P., H. J. J. Jonker, and L. M. Portela, 2009: On the combined effects of turbulence and gravity on droplet collisions in clouds: A numerical study. *Journal of the Atmospheric Sciences*, **66** (7), 1926–1943, doi:10.1175/2005JAS2669.1, <http://dx.doi.org/10.1175/2005JAS2669.1>.
- Zsom, A., and C. P. Dullemond, 2008: A representative particle approach to coagulation and fragmentation of dust aggregates and fluid droplets. *Astron. Astrophys.*, **489** (2), 931–941.